DETC2024-143299

GEOMETRY-DRIVEN DESIGN OF MORPHABLE SURFACE STRUCTURES USING TOPOLOGY OPTIMIZATION AND CIRCLE PACKING

Lingfeng Gao¹, Xiaoping Zhu², Masato Tanaka⁴, Yuyang Song⁴, Yuqing Zhou⁴, Xianfeng David Gu^{2,3},Shikui Chen^{1*}

Department of Mechanical Engineering¹

Department of Computer Science²

Department of Applied Mathematics & Statistics³

State University of New York, Stony Brook, NY, USA, 11794

Toyota Research Institute of North America ⁴, Ann Arbor, MI, USA, 48105

Email: lingfeng.gao@stonybrook.edu; xz349@scarletmail.rutgers.edu; gu@cs.stonybrook.edu; tanamasa@mosk.tytlabs.co.jp; yuyang.song@toyota.com; yuqing.zhou@toyota.com; shikui.chen@stonybrook.edu

ABSTRACT

This paper presents a new computational framework for the co-optimization and co-control of morphable surface structures using topology optimization and circle-packing algorithms. The proposed approach integrates the design of optimized compliant components and the system-level control of the overall surface morphology. By representing the surface shape using circle packing and leveraging conformal mapping, the framework enables smooth deformation between 2D and 3D shapes while maintaining local geometry and global morphology. The morphing surface design problem is recast as designing circular compliant actuators using level-set topology optimization with displacements and stiffness objectives. The optimized component designs are then mapped back onto the circle packing representation for coordinated control of the surface morphology. This integrated approach ensures compatibility between local and global geometries and enables efficient actuation of the morphable surface. The effectiveness of the proposed framework is demonstrated through numerical examples and physical prototypes, showcasing its ability to design and control complex morphable surfaces with applications in various fields. The co-optimization and co-control capabilities of the framework are verified, highlighting its potential for realizing advanced morphable structures with optimized geometries and coordinated actuation. This integrated approach goes beyond conventional methods by considering both local component geometry and global system morphology and enabling coordinated control of the morphable surface. The general nature of our approach makes it applicable to a wide range of problems involving the design and control of morphable structures with complex, adaptive geometries.

Keywords

Morphable Structures. Circle Packing. Conformal Mapping. Compliant Mechanisms. Topology Optimization. Level Set Method. Differential Geometry.

1 INTRODUCTION

Morphable structures capable of transforming into various shapes on demand have garnered significant attention in recent years due to their wide-ranging applications in fields such as soft robotics [15] [7] [13], deployable structures in aerospace engineering [4], and adaptive automotive systems [10]. The ability to design structures that can morph predictably and controllably

^{*}Address all correspondence to this author.

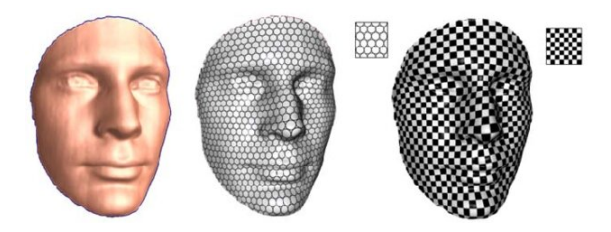


FIGURE 1. PROPERTIES OF CONFORMAL MAPPING (Computational conformal geometry [11])

between target geometries enables novel functionalities and enhances system versatility. However, the rational design and precise control of morphable structures pose significant challenges due to the complex interplay between material properties, structural mechanics, and desired shape transformations.

Topology optimization has emerged as a powerful computational approach for designing structures with optimized material distribution to achieve desired performance objectives [5] [6]. By algorithmically determining the optimal layout of material within a design domain, topology optimization enables the creation of lightweight, high-performance, and multifunctional structures [19] [17]. In the context of morphable structures, topology optimization has been leveraged to design compliant mechanisms and shape-morphing systems. However, existing approaches often struggle to simultaneously maintain precise local geometries and overall shape integrity during the morphing process, limiting their applicability to more complex target geometries. [21] [16]

To address these challenges, we propose a novel framework that synergistically integrates computational conformal geometry and topology optimization for the design of morphable surface structures. Our approach leverages circle packing, a technique for discretely representing surfaces using tangent circles, to model the target morphing behavior. Conformal mapping is then employed to deform the circle-packed surface between 2D and 3D configurations while preserving angle measurements. This conformality ensures that local geometries are maintained even as the global shape undergoes large deformations. By recasting the morphable surface design problem as the design of an interconnected network of circular compliant mechanisms, we enable the application of topology optimization to generate physically realizable structures that can morph into the target geometries.

The main contributions of this work are twofold:

First, we introduce a conformal geometry-driven approach for modeling and controlling the morphing of surface structures based on circle packing and discrete Ricci flow. This mathematical framework provides a principled way to describe and prescribe target morphing behaviors while preserving geometric fidelity. The introduction of circle packing offers several advantages for the kinematic modeling of morphable surface structures. Firstly, circle packing enables an accurate approximation of the surface's local geometry, serving as a valuable tool for shape modeling. Secondly, conformal mapping preserves surface angles, thereby ensuring the overall shape integrity throughout the morphing process. Additionally, Ricci flow refines the surface shape and simulates its temporal evolution, facilitating the creation of highly realistic and dynamic models of morphable surface structures. This methodology proves particularly beneficial for the physical realization of morphable structures using topology optimization, where maintaining both local and overall shape integrity during morphing is imperative for correct structural functionality.

Second, we establish a pipeline for integrating this conformal geometric modeling with topology optimization to automatically generate designs for morphable surface structures that can be fabricated as single-piece compliant mechanisms. The coupling of conformal geometry and topology optimization opens up new possibilities for designing morphable structures with exceptional complexity and precision.

Through circle packing, we translate overall surface morphing into localized changes in the radii of circle packs. This allows us to reformulate the morphable surface design problem as a circular actuator design problem. Consequently, the actuators can expand and contract in edge length and height, corresponding to changes in circle radius and curvature. Following the optimization of a single-piece topology-optimized compliant mechanism, we assemble the circular actuator by revolving the compliant mechanism in a circular direction. Subsequently, the circular actuator is mapped to a circle packing pattern after numerical validation and experimentation, enabling adjustment of circle pack radii to morph the surface shape. Modifying the radii of the circle packing pattern through the proposed circular actuators facilitates the portability and deformability of the surface structure. We have provided several numerical results to support the effectiveness of our methodology.

The rest of the paper is organized as follows: Section 2 introduces the mathematical background on circle packing and conformal geometry that underpins our modeling approach. Section 3 describes our pipeline for integrating conformal geometry with topology optimization and presents the problem formulation. Section 4 details our topology optimization method and sensitivity analysis. Section 5 presents numerical examples and physical prototypes that demonstrate the effectiveness of our approach. Finally, Section 6 discusses the implications of our work and outlines future research directions.

2 CIRCLE PACKING THEORY

Circle packing is a powerful tool from computational geometry that enables the representation of surfaces using a collection

of circles with prescribed tangency relationships [20] [9]. By leveraging the properties of circle packings, such as their ability to capture local geometric information and their shape invariance under conformal transformations, we can develop effective methods for modeling and controlling the morphing of surface structures. In this section, we introduce the key mathematical concepts and theories underlying circle packing-based surface representation and manipulation.

2.1 Koebe-Andreev-Thurston Theorem

The Koebe-Andreev-Thurston Theorem (KAT Theorem) [14] is the fundamental theorem in the circle packing theory. It states that for a finite maximal planar graph G, there exists a circle packing whose tangency graph is isomorphic to G and is unique, up to Möbius transformations and reflections in lines.

The KAT Theorem established a connection between the topology and the geometric realization of a finite graph. Furthermore, it is closely related to the conformal mapping between planar domains. The Riemann mapping theorem, states that, for any two topological disks in the plane, there is a conformal map from one disk to the other. However, it is not easy to construct an explicit conformal mapping between two given domains.

In 1985, Thurston proposed using circle packings to approximate conformal mappings. He suggested filling a domain Ω with a hexagonal tessellation of circles, each of small radius r, and forming a planar graph G from the intersection graph of those circles. The KAT theorem guarantees a circle packing, with the outermost circle as the unit circle, whose tangency graph is isomorphic to G. The resulting discrete conformal mapping is the piecewise linear mapping that preserves the combinatorial structure of G. As shown in Figure 2.1, we can get a sequence of those discrete conformal mappings f_n sending the interior of a region Ω to the unit disk D. Thurston conjectured that as the radius of the tessellation goes to zero, the discrete conformal mappings f_n will converge to the Riemann mapping. This conjecture was confirmed by Rodin and Sullivan in 1987 [18].

2.2 Discrete Ricci Flow and Circle Packing

However, there is no natural analogy for the circle packings on general curved surfaces. Ricci flow on surfaces was first introduced by Hamilton in [12]. Chow and Luo discovered the relations between the Ricci flow and the circle packings and established the theoretical foundation for discrete Ricci flow in [8], where the existence and convergence of the discrete Ricci the flow was established.

Consider M as a two-dimensional, connected, orientable surface, and T is a simplicial *triangulation* of M. Let V(T), E(T), F(T) be the set of vertices, edges, and triangles of T respectively. Furthermore, when M is equipped with a Riemannian metric, T is called a *geodesic triangulation* if every edge in T is a geodesic arc.

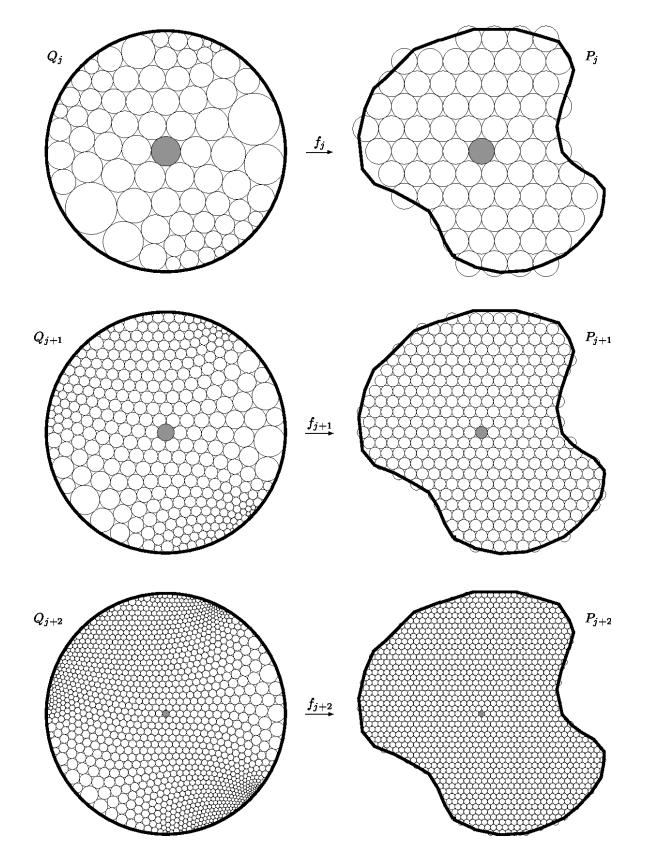


FIGURE 2. Discrete Conformal mappings

Given a triangulation T, if an edge length $l \in \mathbb{R}^{E(T)}_{>0}$ satisfies the triangle inequalities, we can construct a Euclidean polyhedral surface (T,l) by isometrically gluing the Euclidean triangles with the edge lengths defined by l along the pairs of edges. Notice that a Euclidean polyhedral surface exhibits a piecewise Euclidean metric, for a vertex in V(T) could be a singular cone point and the Gaussian curvature is constant 0 at any point not in V(T).

Given $(T,l)_E$, let θ^i_{jk} be the inner angle at the vertex i in the triangle $\triangle ijk$. The *discrete curvature* K_i at the vertex $i \in V(T)$ is defined as

$$K_i = 2\pi - \sum_{jk \in E: \triangle ijk \in F} \theta^i_{jk} \tag{1}$$

A piecewise Euclidean metric is globally flat if and only if $K_i = 0$ for every vertex $i \in V(T)$.

In practice, the objects we study are polyhedral surfaces. Figure 3 shows how the polyhedral surfaces relate to circle packings.

Change infinitesimal circles to circles with finite radii, and each circle is centered at a vertex like a cone, the radius is denoted as γ_i at vertex v_i , and an edge has two vertices, the two

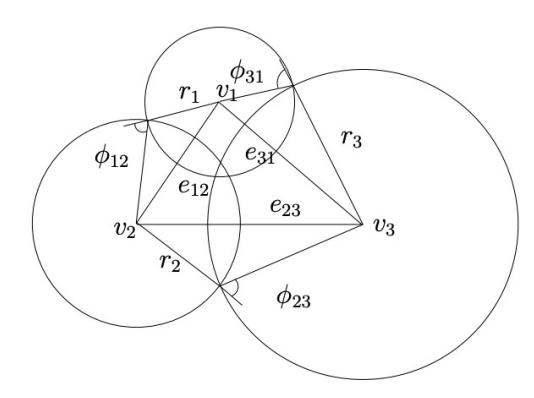


FIGURE 3. **Circle Packing for a metric**: Triangle $[v_1, v_2, v_3]$ has vertices v_1, v_2, v_3 , and edges e_{12}, e_{23}, e_{31} . Three circles centered at v_1, v_2 , and v_3 , with radii r_1, r_2 and r_3 intersect one another, with intersection angles of Φ_{12}, Φ_{23} and Φ_{31} , which are the weights associated with the edges. The edge lengths of the triangle are determined by r_i and Φ_{ij} by the cosine law.

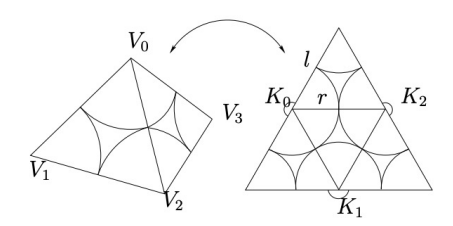


FIGURE 4. Circle packing and cuvature: For a canonical tetrahedron, the edges lengths are all l = 1.0, and the radius at each vertex is r = 0.5. The curvature on each vertex equals to $K_i = \pi$. The weights on all edges are $\Phi = 0$.

circles intersect each other with an intersection angle, the angle is denoted as Φ_{ij} for edge e_{ij} , and called the weight.

Definition 1. A mesh with circle packing (M,Γ,Φ) , where M is the topological triangulation (connectivity), $\Gamma = \{\gamma_i, v_i \in V\}$ are the vertex radii, $\Phi = \{\Phi_{ij}, e_{ij} \in E\}$ are the angles associated with each edge. A discrete conformal mapping $\tau : (M,\Gamma,\Phi) \to (M,\bar{\Gamma},\Phi)$ only changes the vertex radii Γ , but preserves the intersection angles Φ .

In geometric modeling applications, meshes are typically embedded in \mathbb{R}^3 with the metrics induced from the embedding. We can find the optimal weight Φ with initial circle radii Γ , such that the circle packing metric (M, Φ, Γ) is as close as possible to the Euclidean metric in the least square sense. Namely, we want

to determine (M, Φ, Γ) by minimizing the following functional

$$\min_{\Gamma, \Phi} \sum_{e_{ij} \in E} |l_{ij} - \bar{l}_{ij}|^2 \tag{2}$$

where \bar{l}_{ij} is the edge length of e_{ij} in \mathbb{R}^3 .

Then we could utilize the discrete Ricci flow to yield a virtual circle packing realizing the desired curvature.

Definition 2 (Discrete Ricci flow). *The discrete Ricci flow is defined as*

$$\frac{d\gamma_i}{dt} = (\bar{K}_i - K_i)\gamma_i,\tag{3}$$

where \bar{K}_i is the desired discrete curvature.

The discrete Ricci flow is a powerful tool for manipulating circle packings and transforming surface geometries. It operates by adjusting the radii of the circles in a packing based on the difference between their current and target curvatures. The Ricci flow equation (Eq. 3) describes how the radius of each circle evolves over time, with the goal of converging to a packing that realizes the desired curvature distribution.

2.3 Deformation for Surfaces via Circle Packings

As discussed in the last section, given an initial circle packing and the desired curvature for the target metric. We can achieve the target metric through the discrete Ricci flow.

Then Alexandrov convex polyhedron theorem [2], ensures that if the desired curvature at each vertex is positive and the initial circle packing lies on the plane, it is possible to linearly interpolate the curvature to determine the curvature at intermediate steps. Furthermore, the circle packings for those intermediate steps could also be achieved through the discrete Ricci flow. This enables us to outline a deformation process from the initial shape to the target shape via circle packing.

For non-convex target shapes, no theoretical guarantee ensures that the shape at intermediate steps could be embedded in \mathbb{R}^3 . However, satisfactory results can still be achieved provided the initial and target shapes are small.

3 DESIGN OF MORPHABLE SURFACES STRUCTURE3.1 Idea of Morphable Surfaces Structure

The morphable surface structure undergoes deformation from a flat panel to a half sphere, causing simultaneous changes in the radii of individual circles. Circle-packing algorithms yield accurate and precise data for each circle during this transformation. Leveraging this radius data, we aim to devise a mechanism capable of morphing in accordance with the data and adjusting the radii accordingly. It has been observed that the radius changes induced by singular circular units alone are insufficient to achieve the overall transformation from a flat panel to a half sphere. Consequently, there is a growing requirement for the significance of curvature changes brought about by individual circles in this process.

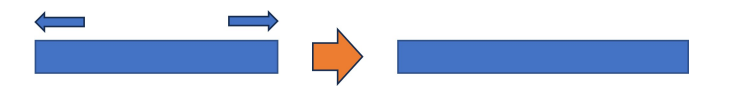


FIGURE 5. EXPANSION IN RADIUS.

Achieving radius changes in a single circular actuator is conceptually straightforward. Illustrated in Figure 5, the fundamental concept involves an expansion and pulley mechanism capable of altering its size while preserving its circular form. This principle finds application in machine gearing adjustments, where dynamic modulation of the pulley radius facilitates changes in gear ratio. The expansion and pulley actuator smoothly adjusts the radius by harnessing motive power, which can be supplied by a motor or similar device.

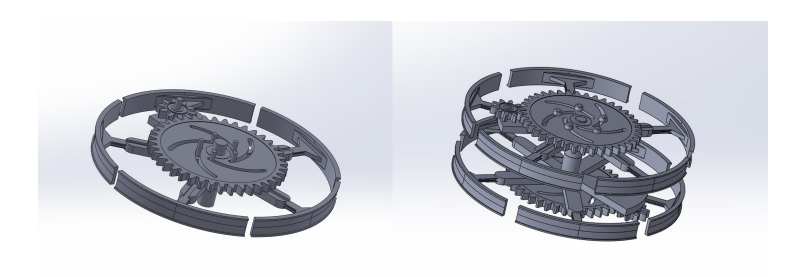


FIGURE 6. SINGLE/DOUBLE EXPANSION AND PULLY MECHANISM.

Achieving curvature changes in a single circular actuator presents a significant challenge, as it involves bending the mechanism to approximate the target curvature. Our innovative approach to not only achieving curvature alterations but also radius changes involves incorporating an additional layer into the mechanism. As depicted in Figure 6, the upper layer of the mechanism expands over a greater distance compared to the lower layer, resulting in a disparity in length between the two layers. This length difference generates curvature when the mechanism comes into contact with another surface. Building upon this concept, we have developed a novel mechanism termed the double

expansion and pulley mechanism, as illustrated in Figure 7.



FIGURE 7. EXPANSION IN RADIUS AND CURVATURE.

The double expansion and pulley mechanism in Figure 7 consists of two concentric circular layers connected by a series of radial spokes. Each layer is composed of a flexible material that can expand or contract in response to an applied force. The outer layer has a slightly larger radius than the inner layer, allowing for differential expansion. The radial spokes ensure that the layers maintain their circular shape during expansion and contraction.

To actuate the mechanism, a set of pulleys and cables are employed. The cables are attached to the outer edge of each layer and routed through the pulleys, which are mounted on a fixed frame surrounding the mechanism. By selectively pulling on the cables, the outer layer can be made to expand more than the inner layer, causing the mechanism to bend and assume a curved shape. The curvature of the mechanism can be controlled by adjusting the relative expansion of the two layers. At the same time, the overall radius of the mechanism can be changed by expanding or contracting both layers simultaneously.



FIGURE 8. THE KEY IDEA OF DOUBLE LAYER MECHANISM EFFECTS THE OVERALL STRUCTURE CURVATURE.

The double expansion and pulley mechanism offers several advantages over alternative designs. First, by using flexible materials and a simple actuation scheme, the mechanism can achieve smooth and controllable curvature changes without the need for complex hinges or joints. Second, the use of concentric layers allows for independent control of radius and curvature, enabling a wide range of target shapes to be realized. Finally, the mechanism can be easily scaled up or down to suit different application

requirements, from small-scale soft robotic components to largescale adaptive structures.

In the context of morphable surface design, the double expansion and pulley mechanism serve as a key building block for realizing the target curvature distributions prescribed by the circle packing-based surface representation. By integrating multiple instances of this mechanism into a larger structure and coordinating their actuation, complex surface geometries can be achieved. The precise control afforded by the mechanism enables the realization of smooth, continuous shape transformations, as required for many morphable surface applications.

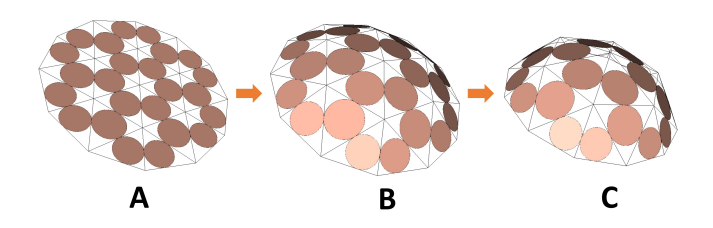


FIGURE 9. CIRCLE PACKING SURFACES FROM FLAT TO HALF SPHERE. (a) initial flat plane with uniform circle radii, (b) intermediate state during Ricci flow with partially adjusted radii, and (c) final deformed semi-spherical surface with target curvatures realized.

3.2 Rigid Body Mechanism v.s. Compliant Mechanism

The rigid body mechanism boasts versatile engineering applications and finds widespread use in manufacturing, robotics, automotive, aerospace, mechanical engineering, and other fields. Its ability to efficiently transmit force and motion between components without undergoing deformation makes it highly desirable. Interconnecting parts via joints facilitate relative motion between them.

While the expansion and pulley mechanism effectively meet design requirements for expanding radii and morphing curvature with stability and precision, larger systems comprising numerous parts may pose increased risks such as buckling and failure.

In contrast, compliant mechanisms offer notable advantages including flexibility, adaptability, lightweight construction, simplified design, and ease of manufacturing. Fabricating compliant mechanisms via 3D printing enables single-piece construction, enhancing convenience and reducing assembly complexity. Employing lightweight single-circular mechanisms may enhance overall system stability.

4 SHAPE AND TOPOLOGY OPTIMIZATION OF COM-PLIANT MECHANISM

4.1 Conventional Level Set Method

Topology optimization, a shape optimization method, employs algorithmic models to optimize material distribution within a predefined design domain, considering specified objective functions, constraints, and boundary conditions. In recent years, topology optimization has garnered increasing popularity and attention within engineering design circles. Its scope has expanded significantly to address a wide array of challenges involving multiphysics coupling, spanning electromagnetics, thermodynamics, acoustics, solid mechanics, and fluid mechanics, among others.

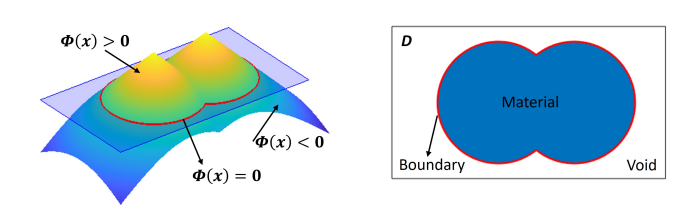


FIGURE 10. A SCHEMATIC OF THE LEVEL SET REPRESENTATION.

The level set method, devised by S. Osher and J.A. Sethian, employs a high-dimensional function to implicitly represent the 2-D contour. Pioneered by Sethian and Wiegmann [1] and further refined by Wang [22] [23] and Allaire [3], this method has emerged as a promising approach for shape and topology optimization. It ensures a clear boundary between phases without a grey region, significantly enhancing precision and optimization accuracy. In this framework, the structural boundary is implicitly represented as the 2-D contour of a level set function with one higher dimension. Implicitly embedded within the level set function $\Phi(\mathbf{x},t)$. Depending on the sign of the level set function, the design domain can be partitioned into three distinct regions, representing the material, the interface, and the void, respectively, as follows:

$$\begin{cases} \Phi(\mathbf{x},t) > 0, & x \in \Omega, & \text{Material} \\ \Phi(\mathbf{x},t) = 0, & x \in \partial\Omega, & \text{Boundary} \\ \Phi(\mathbf{x},t) < 0, & x \in D/\Omega, & \text{Void} \end{cases}$$
 (4)

where D denotes the design domain. The evolution of the boundary dynamics is governed by the Hamilton-Jacobi equation:

$$\frac{\partial \Phi(\mathbf{x},t)}{\partial t} - V_n \cdot |\nabla \Phi(\mathbf{x},t)| = 0, \tag{5}$$

The normal velocity field V_n can be determined through shape sensitivity analysis. Solving the Hamilton-Jacobi equation outlined above enables the updating of the normal velocity field, which subsequently governs the evolution of the structural boundary.

4.2 Problem Formulation

The objective of the topology optimization problem for the single-piece compliant actuator is twofold: (1) kinematic performance: minimizing the discrepancy between the target and actual deformation of the actuator and (2) load-carrying capability: maximizing the structural stiffness while maintaining a prescribed volume fraction. The problem can be mathematically formulated as follows:

Minimize:
$$J = \omega_1 \left(\int_{\Omega} \varepsilon_{ij}(\boldsymbol{u}) E_{ijkl} \varepsilon_{kl}(\boldsymbol{u}) d\Omega \right)$$
$$+ \omega_2 \left(\int_{\Omega} k |\boldsymbol{u} - \boldsymbol{u}_0|^{\alpha} d\Omega \right)^{\frac{1}{\alpha}},$$
$$\alpha = 2$$
Subject to:
$$a(\boldsymbol{u}, \boldsymbol{v}) = l(\boldsymbol{v}), \quad \forall \, \boldsymbol{v} \in U$$
$$V(\Omega) = V^*.$$

where u is the state variable (displacement) in the admissible displacement space; Ω is the design variable which is the shape of the material region in the design domain; D represents the design domain; ε_{ij} is the strain tensor; E_{ijkl} is the elasticity tensor; u_0 is the target displacement; k is a weighting factor; ω_1 and ω_2 are weighting coefficients for the stiffness and displacement objectives, respectively; a(u,v) and l(v) are the energy bilinear form and the load linear form, respectively; U is the space of admissible displacements; V^* is the prescribed volume fraction.

The first term in the objective functional J represents the structural stiffness, while the second term measures the discrepancy between the actual and target displacements using an L^{α} -norm. The parameter α is set to 2, resulting in a quadratic penalty for deviations from the target displacement.

The constraint a(u,v)=l(v) ensures that the displacement field satisfies the governing equations of linear elasticity. The volume constraint $V(\Omega)=\int_{\Omega}H(\phi)d\Omega=V^*$. limits the amount of material that can be used in the design. k is a region indicator, which equals 1 inside a specific region and 0 outside [3].

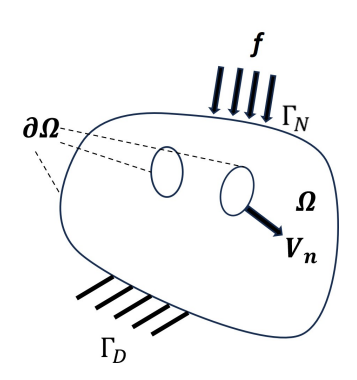


FIGURE 11. A SCHEMATIC OF GENERAL BOUNDARY CONDITION.

4.3 Shape Sensitivity Analysis

The topology optimization problem for the single-piece soft actuator can be formulated as a PDE-constrained optimization problem. To solve this problem, the Lagrange multipliers method is utilized to transform the PDE-constrained problem into an unconstrained optimization problem. This is achieved by defining the Lagrangian functional L as follows, which integrates the objective function and governing equation with a Lagrange multiplier λ .

$$L = J + \lambda (a(\mathbf{u}, \mathbf{v}) - l(\mathbf{v})), \tag{7}$$

where J is the objective functional, a(u,v) represents the weak form of the governing equations, and l(v) is the load functional.

4.3.1 Adjoint Equation Derivation: To derive the adjoint equation, we take the variation of the Lagrangian functional L with respect to the state variable \mathbf{u} and the Lagrange multiplier λ :

Setting $\delta L = 0$ leads to the adjoint equation:

$$a(u',v) = -\frac{\delta J}{\delta u} \tag{8}$$

where v is the adjoint variable and u' is the test function. As for this problem, the total derivative of the objective func-

As for this problem, the total derivative of the objective function and governing equation is as follows:

$$\frac{DL}{Dt} = \frac{DJ}{Dt} + \frac{Da(\mathbf{u}, \mathbf{v})}{Dt} - \frac{Dl(\mathbf{v})}{Dt}$$
(9)

The material time derivative of the objective function is formulated as:

$$\frac{\partial L}{\partial t} = \frac{\partial J}{\partial t} + \frac{\partial J}{\partial \Omega}
\frac{\partial J}{\partial t} = 2\omega_{1} \left(\int_{\Omega} \varepsilon_{ij}(\mathbf{u}') E_{ijkl} \varepsilon_{kl}(\mathbf{u}) d\Omega \right)
+ \omega_{2} \left(\int_{\Omega} k |\mathbf{u} - \mathbf{u}_{0}|^{2} d\Omega \right)^{-\frac{1}{2}} \cdot \int_{\Omega} k (\mathbf{u} - \mathbf{u}_{0}) \cdot \mathbf{u}' d\Omega$$

$$\frac{\partial J}{\partial \Omega} = \omega_{1} \left(\int_{\Omega} \varepsilon_{ij}(\mathbf{u}) E_{ijkl} \varepsilon_{kl}(\mathbf{u}) V_{n} ds \right)
+ \frac{\omega_{2}}{2} \left(\int_{\Omega} k |\mathbf{u} - \mathbf{u}_{0}|^{2} d\Omega \right)^{-\frac{1}{2}} \cdot \int_{\partial \Omega} k (\mathbf{u} - \mathbf{u}_{0})^{2} \cdot V_{n} ds$$
(10)

The material time derivative of the energy form and the load form can be expressed as:

$$\frac{Da(\boldsymbol{u},\boldsymbol{v})}{Dt} = \frac{\partial a(\boldsymbol{u},\boldsymbol{v})}{\partial t} + \frac{\partial a(\boldsymbol{u},\boldsymbol{v})}{\partial \Omega}
\frac{\partial a(\boldsymbol{u},\boldsymbol{v})}{\partial t} = \int_{\Omega} \varepsilon_{ij}(\boldsymbol{u}') E_{ijkl} \varepsilon_{kl}(\boldsymbol{v}) d\Omega
+ \int_{\Omega} \varepsilon_{ij}(\boldsymbol{u}) E_{ijkl} \varepsilon_{kl}(\boldsymbol{v}') d\Omega
\frac{\partial a(\boldsymbol{u},\boldsymbol{v})}{\partial \Omega} = \int_{\Omega} \varepsilon_{ij}(\boldsymbol{u}) E_{ijkl} \varepsilon_{kl}(\boldsymbol{v}) V_n ds$$
(11)

Where v is the adjoint displacement,

$$\frac{Dl(\mathbf{v})}{Dt} = \frac{\partial l(\mathbf{v})}{\partial t} + \frac{\partial l(\mathbf{v})}{\partial \Omega}
= \int_{\Omega} \mathbf{g} \cdot \mathbf{v}' d\Omega + \int_{\Gamma_N} \mathbf{f} \cdot \mathbf{v}' d\Gamma_N
+ \int_{\partial \Omega} \mathbf{g} \cdot \mathbf{v} V_n ds
+ \int_{\partial \Omega} \left[\frac{\partial (\mathbf{f} \cdot \mathbf{v})}{\partial n} + k(\mathbf{f} \cdot \mathbf{v}) V_n \right] ds$$
(12)

Here, the total derivative can be rewritten as:

$$\frac{DL}{Dt} = 2\omega_{1} \left(\int_{\Omega} \varepsilon_{ij}(\mathbf{u}') E_{ijkl} \varepsilon_{kl}(\mathbf{u}) d\Omega \right)
+ \omega_{2} \left(\int_{\Omega} k |\mathbf{u} - \mathbf{u}_{0}|^{2} d\Omega \right)^{-\frac{1}{2}} \cdot \int_{\Omega} k (\mathbf{u} - \mathbf{u}_{0}) \cdot \mathbf{u}' d\Omega
+ \omega_{1} \left(\int_{\Omega} \varepsilon_{ij}(\mathbf{u}) E_{ijkl} \varepsilon_{kl}(\mathbf{u}) V_{n} ds \right)
+ \frac{\omega_{2}}{2} \left(\int_{\Omega} k |\mathbf{u} - \mathbf{u}_{0}|^{2} d\Omega \right)^{-\frac{1}{2}} \cdot \int_{\partial\Omega} k (\mathbf{u} - \mathbf{u}_{0})^{2} \cdot V_{n} ds
+ \int_{\Omega} \varepsilon_{ij}(\mathbf{u}') E_{ijkl} \varepsilon_{kl}(\mathbf{v}) d\Omega + \int_{\Omega} \varepsilon_{ij}(\mathbf{u}) E_{ijkl} \varepsilon_{kl}(\mathbf{v}') d\Omega
+ \int_{\Omega} \varepsilon_{ij}(\mathbf{u}) E_{ijkl} \varepsilon_{kl}(\mathbf{v}) V_{n} ds - \int_{\Omega} \mathbf{g} \cdot \mathbf{v}' d\Omega
- \int_{\Gamma_{N}} \mathbf{f} \cdot \mathbf{v}' d\Gamma_{N} - \int_{\partial\Omega} \mathbf{g} \cdot \mathbf{v} V_{n} ds
- \int_{\partial\Omega} \left[\frac{\partial (\mathbf{f} \cdot \mathbf{v})}{\partial n} + k (\mathbf{f} \cdot \mathbf{v}) V_{n} \right] ds$$
(13)

Solve Adjoint Equation,

$$2\omega_{1} \left(\int_{\Omega} \varepsilon_{ij}(\mathbf{u}') E_{ijkl} \varepsilon_{kl}(\mathbf{u}) d\Omega \right)$$

$$+ \omega_{2} \left(\int_{\Omega} k |\mathbf{u} - \mathbf{u}_{0}|^{2} d\Omega \right)^{-\frac{1}{2}} \cdot \int_{\Omega} k (\mathbf{u} - \mathbf{u}_{0}) \cdot \mathbf{u}' d\Omega$$

$$+ \int_{\Omega} \varepsilon_{ij}(\mathbf{u}') E_{ijkl} \varepsilon_{kl}(\mathbf{v}) d\Omega$$

$$(14)$$

Let $D_0 = (\int_{\Omega} k |\mathbf{u} - \mathbf{u}_0|^2 d\Omega)^{-\frac{1}{2}}$, then we can write the above equation as

$$\int_{\Omega} \varepsilon_{ij}(\mathbf{u}') E_{ijkl} \varepsilon_{kl}(\mathbf{v}) d\Omega =$$

$$- \omega_2 D_0 \cdot \int_{\Omega} k(\mathbf{u} - \mathbf{u}_0) \cdot \mathbf{u}' d\Omega \qquad (15)$$

$$- 2\omega_1 \left(\int_{\Omega} \varepsilon_{ij}(\mathbf{u}') E_{ijkl} \varepsilon_{kl}(\mathbf{u}) d\Omega \right)$$

Since

$$\int_{\Omega} \boldsymbol{\varepsilon}_{ij}(\boldsymbol{u}') E_{ijkl} \boldsymbol{\varepsilon}_{kl}(\boldsymbol{u}) \, \mathrm{d}\Omega = \int_{\Omega} \boldsymbol{g} \cdot \boldsymbol{u}' \, \mathrm{d}\Omega + \int_{\Gamma_N} \boldsymbol{f} \cdot \boldsymbol{u}' \, \mathrm{d}\Gamma_N \quad (16)$$

$$\int_{\Omega} \varepsilon_{ij}(\mathbf{u}') E_{ijkl} \varepsilon_{kl}(\mathbf{v}) d\Omega =
- \omega_{2} D_{0} \cdot \int_{\Omega} k(\mathbf{u} - \mathbf{u}_{0}) \cdot \mathbf{u}' d\Omega - 2\omega_{1} \int_{\Omega} \mathbf{g} \cdot \mathbf{u}' d\Omega
- 2\omega_{1} \int_{\Gamma_{N}} \mathbf{f} \cdot \mathbf{u}' d\Gamma_{N}
\int_{\Omega} \varepsilon_{ij}(\mathbf{u}') E_{ijkl} \varepsilon_{kl}(\mathbf{v}) d\Omega =
\int_{\Omega} (-\omega_{2} D_{0} \cdot k(\mathbf{u} - \mathbf{u}_{0}) - 2\omega_{1} \mathbf{g}) \cdot \mathbf{u}' d\Omega +
\int_{\Gamma_{N}} (-2\omega_{1} \cdot \mathbf{f}) \cdot \mathbf{u}' d\Gamma_{N}$$
(17)

The strong form of the adjoint solution is as follows:

$$-\nabla \cdot \boldsymbol{\sigma}(\boldsymbol{v}) = -\omega_2 D_0 \cdot k(\boldsymbol{u} - \boldsymbol{u}_0) - 2\omega_1 \boldsymbol{g}, \text{ on } \Omega,$$

$$\boldsymbol{v} = 0, \text{ on } \Gamma_D,$$

$$\boldsymbol{\sigma}(\boldsymbol{v}) \cdot \boldsymbol{n} = -2\omega_1 \cdot \boldsymbol{f}, \text{ on } \Gamma_N,$$
(18)

4.3.2 Construction of Design Velocity: Once the adjoint equation is solved, the design velocity V_n can be calculated using the following expressions. In this work, the body force \mathbf{g} is not considered in the problem:

$$\omega_{1} \left(\int_{\partial \Omega} \varepsilon_{ij}(\boldsymbol{u}) E_{ijkl} \varepsilon_{kl}(\boldsymbol{u}) V_{n} \, \mathrm{d}s \right)$$

$$+ \frac{\omega_{2}}{2} \left(\int_{\Omega} k |\boldsymbol{u} - \boldsymbol{u}_{0}|^{2} \, \mathrm{d}\Omega \right)^{-\frac{1}{2}} \cdot \int_{\partial \Omega} k (\boldsymbol{u} - \boldsymbol{u}_{0})^{2} \cdot V_{n} \, \mathrm{d}s$$

$$+ \int_{\partial \Omega} \varepsilon_{ij}(\boldsymbol{u}) E_{ijkl} \varepsilon_{kl}(\boldsymbol{v}) V_{n} \, \mathrm{d}s$$

$$(19)$$

With the steepest descent method, the normal design velocity can be constructed as

$$V_{n1} = -\omega_1 \varepsilon_{ij}(\mathbf{u}) E_{ijkl} \varepsilon_{kl}(\mathbf{u})$$

$$V_{n2} = -\frac{\omega_2}{2} D_0 k(\mathbf{u} - \mathbf{u}_0)^2$$

$$V_{n3} = -\varepsilon_{ij}(\mathbf{u}) E_{ijkl} \varepsilon_{kl}(\mathbf{v})$$
(20)

The total design velocity V_n is then obtained by summing these three components:

$$V_n = -\omega_1 \varepsilon_{ij}(\mathbf{u}) E_{ijkl} \varepsilon_{kl}(\mathbf{u}) - \frac{\omega_2}{2} D_0 k(\mathbf{u} - \mathbf{u}_0)^2 - \varepsilon_{ij}(\mathbf{u}) E_{ijkl} \varepsilon_{kl}(\mathbf{v})$$
(21)

This design velocity is used to evolve the structural boundary and optimize the topology of the compliant actuator.

5 NUMERICAL EXAMPLES

5.1 Topology Optimization of Single-piece compliant actuator

This example is to find the optimum design of the singlepiece compliant actuator, as figure 10 shows, the boundary conditions of the single-piece actuator are the Input force at the top left, roller constraints at the left edge, and fixed constraints at the bottom left. Two blue squares indicate the kinematic region, and the two red squares indicate the target position the kinematic region tries to approach. The target position is determined by the circle packing algorithms. Based on the data generated, we can find the corresponding radii and the curvature target of every single circular actuator can be found from the overall radii. The window factor k is zero except in the blue zone where it is equal to 1. The force applied is 3 Newton. The material used in this example is a dummy material with Young's modulus E = 1000Pa, the Poisson's ratio is given by 0.3, and the density is 1. The weighting factor of this topology optimization problem is $w_1 =$ $0.0042, w_2 = 0.9958.$

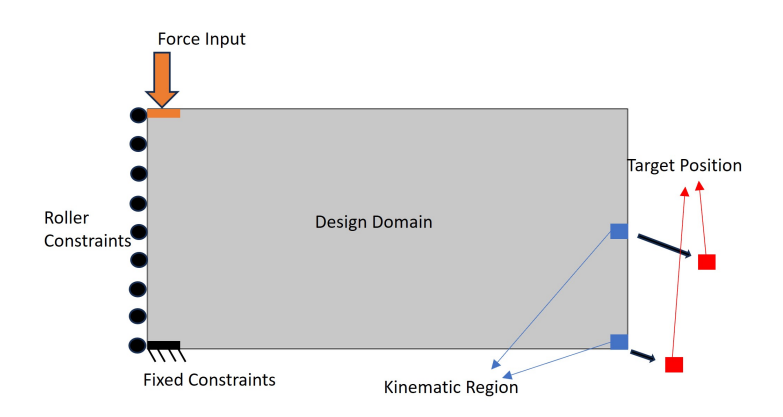


FIGURE 12. BOUNDARY CONDITIONS OF THE SINGLE-PIECE ACTUATOR

The entire design domain is discretized into a grid of 100×50 grids. Both constituent materials are constrained to occupy 30

percent of the total volume. Figure 11 depicts the convergence curve of the optimization process and the history of design evolution. The optimization process involves a total of 2000 iterations.

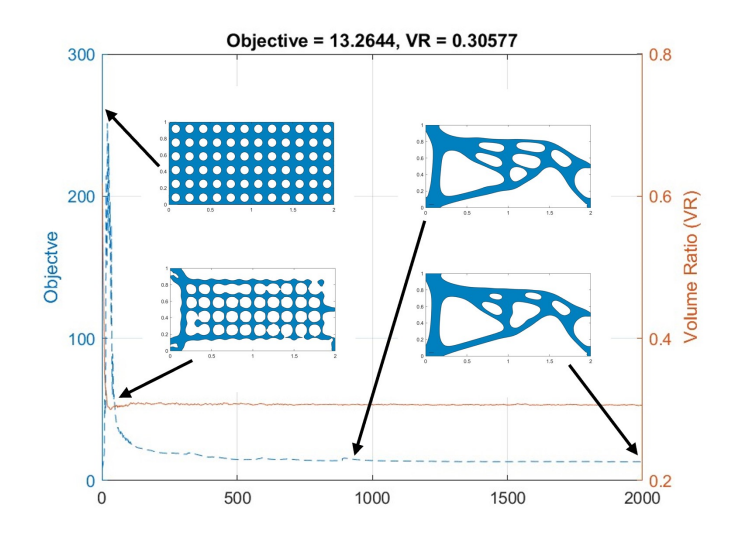


FIGURE 13. THE TOPOLOGY OPTIMIZATION HISTORY PLOT.

Following 2000 iterations of evolution, the optimization outcome is depicted in Figure 12. Material regions are represented in blue, while void regions are displayed in white. In this numerical example, finite element analysis is carried out to verify the optimization results, with boundary conditions applied to the optimized outcome. The verification results are illustrated in Figure 13. A downward force of 3 Newton is applied at the top left, and the kinematic region converges toward the target position. The final volume ratio is 30 percent.

The single-piece soft actuator successfully meets the design criteria following verification. Utilizing symmetry, the single-circular actuator is constructed from the circular pattern of single-piece actuators. Six single-piece actuators are assembled to form one circular actuator. Figure 14 depicts the single circular actuator and its verification, which is conducted via finite element analysis. A force is applied to the top of the circular actuator, resulting in the bending and expansion of the entire structure according to the designed curvature and radius. In future physical experiments, the force could be generated by a motor or similar device.

5.2 System Analysis of The Entire Circular Packing System

The complete morphable surface structure comprises 24 single circular actuators, with each single circular actuator constructed from 6 single-piece actuators. Once assembled, as de-

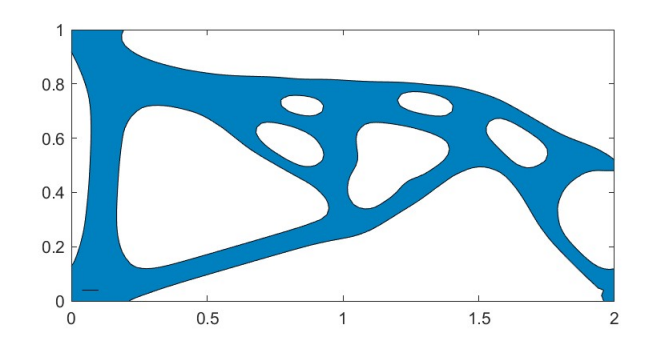


FIGURE 14. FINAL RESULT OF THE TOPOLOGY-OPTIMIZED COMPLIANT ACTUATOR.

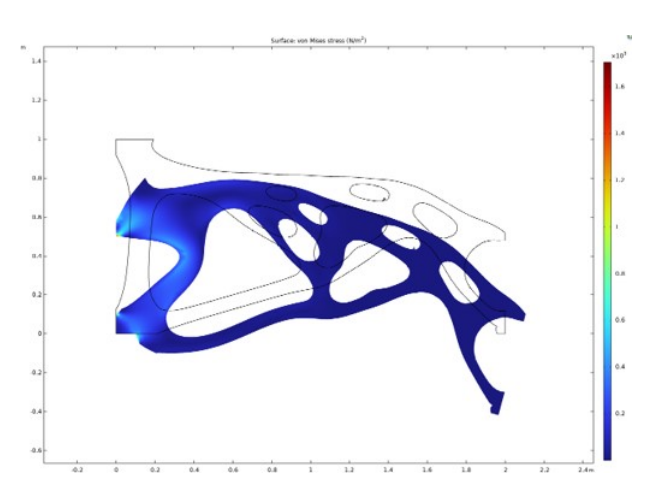


FIGURE 15. NUMERICAL VALIDATION OF THE MORPHING BEHAVIOR OF THE COMPLIANT ACTUATOR DESIGNED USING TOPOLOGY OPTIMIZATION.

picted in Figure 16, the curvature and radius of the entire structure are validated against the graph in Figure 15, generated through circle packing algorithms. The verification of the single-piece actuator was conducted using finite element analysis, and similarly, the single circular actuator assembled from the single-piece actuators underwent verification via finite element analysis. Once the verification of the single circular actuator is completed, it can be integrated into the overall morphable surface structure.

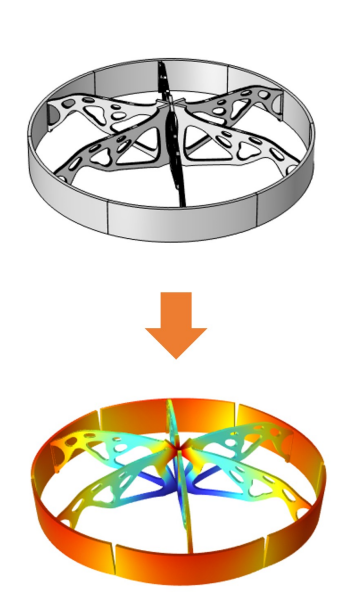


FIGURE 16. NUMERICAL VERIFICATION OF THE BEHAVIOR OF A CIRCULAR COMPLAINT ACTUATOR ASSEMBLY.

6 DISCUSSIONS AND CONCLUSIONS

This paper presents a new approach for achieving cooptimization and co-design morphable structures utilizing circlepacking theory and topology optimization to design individual single-piece structures. The main contributions of this work lie in the development of a computational framework that integrates topology optimization and circle-packing algorithms for the cooptimization and co-control of morphable surface structures and the demonstration of its effectiveness through a benchmark numerical example. This integrated approach goes beyond conventional methods by considering both local component geometry and global system morphology and enabling coordinated control of the morphable surface.

The morphing behavior of the single circular actuator is driven by a downward input force applied at the center. While we simplify the problem at the current stage by assuming linear elasticity, it is acknowledged that the soft material exhibits nonlinear elasticity. As for the single circular actuator integrated into the overall structure, assembly involves reconfiguring them from a flat panel to a half sphere. Future efforts will focus on achieving fully automated simulation, enabling seamless morphing from a flat panel to a half sphere without manual intervention. Additionally, experiments and physical validations will be conducted to validate the proposed approach.

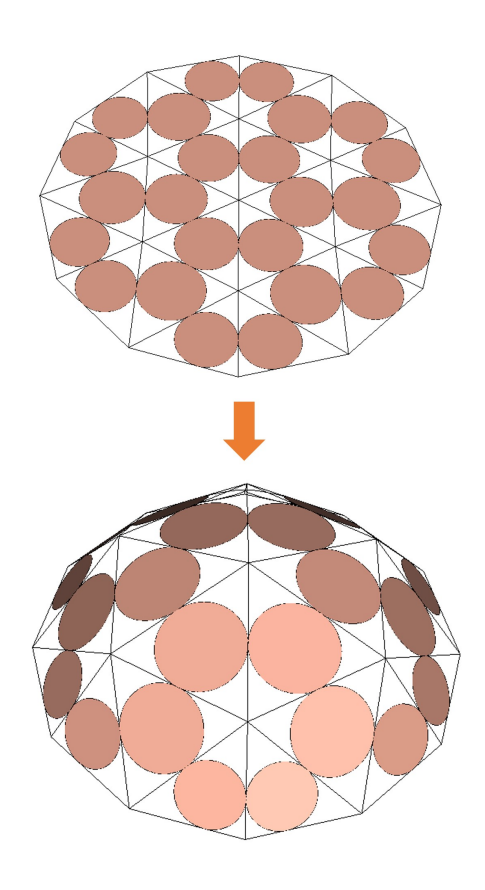


FIGURE 17. TRANSFORMATION OF A FLAT SURFACE INTO A COMPLEX 3D GEOMETRY THROUGH CIRCLE PACKING-BASED MORPHABLE DESIGN.

ACKNOWLEDGMENT

This work was supported in part by the National Science Foundation under grants CMMI-1762287 and PFI-RP-2213852, and by Toyota Research Institute of North America under award 93761.

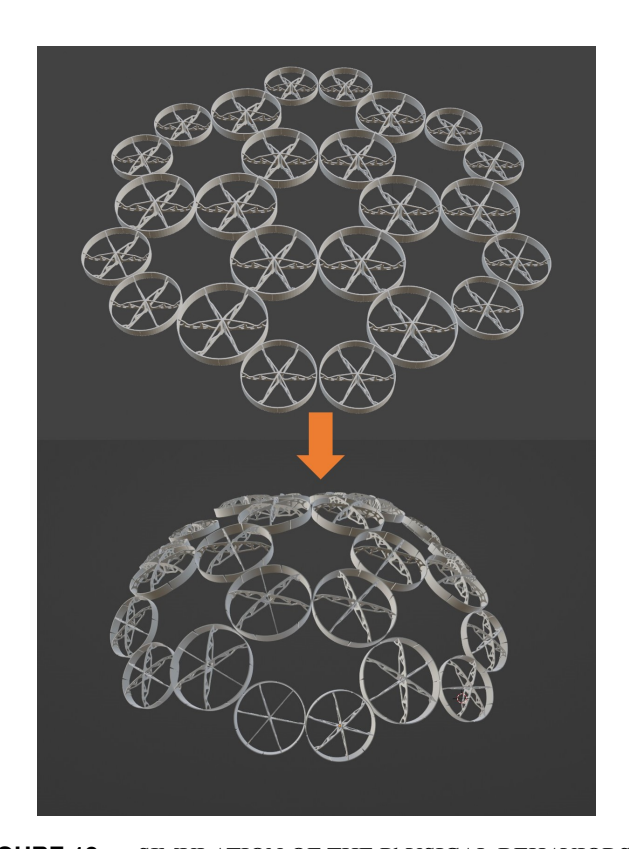


FIGURE 18. SIMULATION OF THE PHYSICAL BEHAVIORS of THE CIRCLE-PACKING MORPHABLE SURFACES STRUCTURE.

REFERENCES

- [1] Structural boundary design via level set and immersed interface methods. *Journal of Computational Physics*, 163(2):489–528, 2000.
- [2] A. D. Alexandrov. Existence of a convex polyhedron and of a convex surface with a given metric. *Matematicheskii Sbornik, New Series*, 11(53):15–65, 1942.
- [3] Grégoire Allaire, François Jouve, and Anca-Maria Toader. Structural optimization using sensitivity analysis and a level-set method. *Journal of computational physics*, 194(1):363–393, 2004.
- [4] Peter Belobaba, Jonathan Cooper, Roy Langton, and Allan Seabridge. *Morphing aerospace vehicles and structures*, volume 57. John Wiley & Sons, 2012.
- [5] Martin P Bendsøe and Ole Sigmund. Material interpolation schemes in topology optimization. *Archive of applied mechanics*, 69:635–654, 1999.
- [6] Martin Philip Bendsoe and Ole Sigmund. *Topology optimization: theory, methods, and applications*. Springer Science & Business Media, 2013.
- [7] Qianying Chen, Fan Feng, Pengyu Lv, and Huiling Duan. Origami spring-inspired shape morphing for flexible robotics. *Soft Robotics*, 9(4):798–806, 2022.
- [8] B. Chow and F. Luo. Combinatorial ricci flows on surfaces. *Journal of Differential Geometry*, 63(1):97–129, 2003.
- [9] Bennett Chow, Sun-Chin Chu, David Glickenstein, Christine Guenther, Jim Isenberg, Tom Ivey, Dan Knopf, Peng Lu, Feng Luo, and Lei Ni. *The Ricci flow: techniques and applications*, volume 135. American Mathematical Society Providence, 2007.
- [10] Urban Fasel, Dominic Keidel, Leo Baumann, Giovanni Cavolina, Martin Eichenhofer, and Paolo Ermanni. Composite additive manufacturing of morphing aerospace structures. *Manufacturing Letters*, 23:85–88, 2020.
- [11] Xianfeng David Gu and Shing Tung Yau. Computational conformal geometry. (*No Title*), 2008.
- [12] R. S. Hamilton. The ricci flow on surfaces. In *Mathematics and General Relativity*, volume 71 of *Contemporary Mathematics*, Providence, RI, 1988. American Mathematical Society. Santa Cruz, CA, 1986.
- [13] Michael Ishida, Dylan Drotman, Benjamin Shih, Mark Hermes, Mitul Luhar, and Michael T Tolley. Morphing structure for changing hydrodynamic characteristics of a soft underwater walking robot. *IEEE Robotics and Automation Letters*, 4(4):4163–4169, 2019.
- [14] P. Koebe. *Kontaktprobleme der konformen Abbildung*. Hirzel, 1936.
- [15] Ke Liu, Felix Hacker, and Chiara Daraio. Robotic surfaces with reversible, spatiotemporal control for shape morphing and object manipulation. *Science Robotics*, 6(53):eabf5116, 2021.
- [16] Junzhao Luo, Zhen Luo, Shikui Chen, Liyong Tong, and

- Michael Yu Wang. A new level set method for systematic design of hinge-free compliant mechanisms. *Computer Methods in Applied Mechanics and Engineering*, 198(2):318–331, 2008.
- [17] Zhen Luo, Michael Yu Wang, Shengyin Wang, and Peng Wei. A level set-based parameterization method for structural shape and topology optimization. *International Journal for Numerical Methods in Engineering*, 76(1):1–26, 2008.
- [18] Burton Rodin and Dennis Sullivan. The convergence of circle packings to the riemann mapping. *Journal of Differential Geometry*, 26:349–360, 1987.
- [19] Ole Sigmund and MP Bondsgc. Topology optimization. State-of-the-Art and Future Perspectives, Copenhagen: Technical University of Denmark (DTU), 2003.
- [20] Kenneth Stephenson. *Introduction to circle packing: The theory of discrete analytic functions*. Cambridge University Press, 2005.
- [21] Jiawei Tian, Manqi Li, Zhonghao Han, Yong Chen, Xianfeng David Gu, QJ Ge, and Shikui Chen. Conformal topology optimization of multi-material ferromagnetic soft active structures using an extended level set method. *Computer Methods in Applied Mechanics and Engineering*, 389:114394, 2022.
- [22] Michael Yu Wang and Xiaoming Wang. "color" level sets: a multi-phase method for structural topology optimization with multiple materials. *Computer Methods in Applied Mechanics and Engineering*, 193(6):469–496, 2004.
- [23] Shengyin Wang and Michael Yu Wang. Radial basis functions and level set method for structural topology optimization. *International journal for numerical methods in engineering*, 65(12):2060–2090, 2006.